# A PIV study of the cerebrospinal fluid dynamics inside a model of the human ventricular system

by

S. Ammourah [(1)], A. Aroussi [(1)] and M. Vloeberghs [(2)]

[(1)] University of Nottingham

School of Mechanical, material, manufacturing Engineering and management

University park, NG7 2RD, Nottingham, UK.

[(2)] Queens medical centre

Department of child health

Nottingham, NG7 2UH, UK.

[(1)]E-Mail: eaxsaka@nottingham.ac.uk

[(2)]E-Mail: Michael.Vloeberghs@nottingham.ac.uk

## ABSTRACT

The Cerebrospinal fluid (CSF) is a biomedical fluid contained within the cerebral ventricles and the subarachnoid space deep inside the human brain. The CSF has a major role as a damper that protects the head from injuries and transports biochemical elements and proteins inside the brain. The CSF flow is a complex phenomenon due to the complexity of the ventricular system shape and the external parameters that are affecting the CSF flow such as the cardiac and respiratory cycles. Furthermore, it is considered as a creep flow due to its low production rate, which is between 100-500 *ml/day*. It has become essential to comprehend the CSF flow dynamics, which is poorly understood, as this knowledge can be manipulated to understand the injected drugs behaviour as a second phase in the CSF continuum. Due to the irregularity and complexity of the ventricular system, a simplified representative geometry was built. The dimensions of the ventricular system have been taken from the MRI scan data and utilized to construct both numerical and experimental models. The computational model has the same volume as the real geometry, but the experimental model was scaled up to 4:1 of the real geometry due to the presence of tiny passages such as the aqueduct, which has a diameter of 1.4 mm. Numerically, different CSF flow rates were studied using the commercial CFD code Fluent 6.1. Experimentally, a pulsed laser system is used to investigate the flow inside the physical rig, using the PIV technique. The PIV system consists of frequency doubled pulsed Nd: YAG laser (532 nm- a green wavelength), a CCD camera sensitive to blue/green spectrum and seeding particles. The Polyamide Seeding Particles (PSP-20), 20 $\mu m$ diameter and 250 g were used in a water continuum. The PIV results show a significant matching with the CFD results and it emphasised the presence of a recirculation motion everywhere in the model. The PIV results show that the highest velocity in the lateral ventricles exists near the inlets and the highest velocities in the entire model occur in the aqueduct.

## 1. GENERAL BACKGROUND

The ventricular system in the human brain consists of four main cerebral chambers; the two lateral ventricles, the 3$^{rd}$ ventricle, and the forth ventricle. The lateral ventricles communicate with the 3$^{rd}$ ventricle via the Foramens of Monro (F.O.M), which are two tiny cylindrical passages connected to the lateral ventricle. The 3$^{rd}$ ventricle communicates with the 4$^{th}$ ventricle via the aqueduct of Sylvius, which is a tiny cylindrical passage as well. Figure 1 illustrates the human ventricular system.

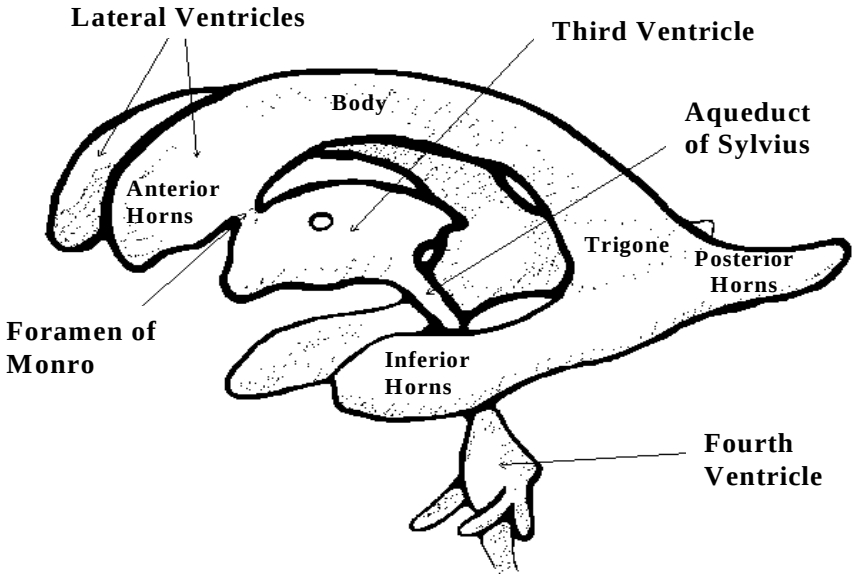


*Fig. 1. Schematic diagram of the real human ventricular system.*

Cerebrospinal fluid (CSF) is the fluid that is secreted from the Choroids plexus, which is a collective group of cells responsible for the CSF secretion and mainly exists at the bottom of the lateral ventricles, but less than 40% at the roof of the 3rd ventricle. The CSF fills the ventricular compartments and flows from the lateral ventricles to the 4th ventricle and then exits to the spinal sac (Proescholdt et al, 2000). The CSF is contained within the cerebral ventricles and the subarachnoid spaces. The CSF is considered as a Newtonian and incompressible fluid. The density of the CSF ranges between 1005-1007 kg/m$^3$ depending on the presence of some proteins and blood cells, and it has a viscosity of 0.00084kg/m-s at normal body temperature (Bloomfield et al, 1998). The CSF flow rate ranges between 100-500*ml/day* (Vloeberghs et al, 2000).

Understanding the CSF is an increasingly important area, because of its usefulness as a drug carrier to treat the brain tumours bypassing the barriers such as the Blood-Brain barrier (BBB) (Siegal & Zylber-Katz, 2002). Based on that, comprehension of such flow is essential for the improvement of chemotherapeutic drugs.

The non-intrusive diagnostic techniques such as the PIV has proven its utility in studying in vitro models of different bio-fluidics such as the blood flows, heart pumps and medicine inhalers. The pulsatile flow in cerebrovascular aneurysm models (Yu et al, 1997) gave a good example of the PIV application in a medical problem.

## 2. EXPERIMENTAL METHODOLOGY

### 2.1 Model Construction

The dimensions of the ventricular system are taken from the MRI scans of the co-author and utilised to construct a 3-D model of the ventricular system, which is then exported to AutoCAD to construct a 3-D computational model (Aroussi et al, 2000). The dimensions obtained from the 3-D real numerical model are manipulated to create the 3-D simplified model for both experiments and computations.

The idea of the simplified model had been explored because of the complexity and irregularity of the ventricular system geometry, which make it very difficult to mimic the macro features of the cerebral ventricles. The design is based on the numerical findings of different studies conducted on 2-D and 3-D numerical models of the ventricular system. These findings are the presence of three distinct pressure regions descending from high pressure at the lateral ventricles and a comparatively low pressure at the 4th ventricle, as well as the existence of dead regions in the lateral ventricles, which are considered as fluid entrapments (Zainy, 2002, Aroussi et al 2000 and Ammourah et al, 2003). These dead regions are excluded from the simplified design. These parts are the posterior horns and the inferior horns shown in figure 1. The lateral ventricles are re-constructed as two rectangular compartments with a separation wall in between. The real

dimensions of each lateral ventricle are 36.5, 45.5 and 93.94 *mm* in the X, Y and Z respectively. The 3rd ventricle is also modelled as a rectangular chamber with dimensions of 5.12, 12 and 31 *mm* in the X, Y and Z directions. The aqueduct of Sylvius is simplified to a cylinder of 1.4*mm* in diameter, and 11*mm* in height. The lowest chamber of the ventricular system is the 4th ventricle, which is also modelled as a cylinder with dimensions of 18.3*mm* in diameter (this value is the average value of the two diameters of the 4th ventricle), and 23*mm* in height. The Foramens of Monro are modelled as small cylinders, three on each side and very close together. They have a total volume as the real Foramen, which is a volume of a cylinder of 1.5 *mm* diameter and 1 *mm* height for each side. All these dimensions are scaled up to 4:1 for the experimental model to ease the visualisation due to the presence of tiny passages such as the aqueduct, but taking the dynamic similarities into account. Figure 2 shows the simplified model drawn by AutoCAD, while figure 3 shows the physical rig.

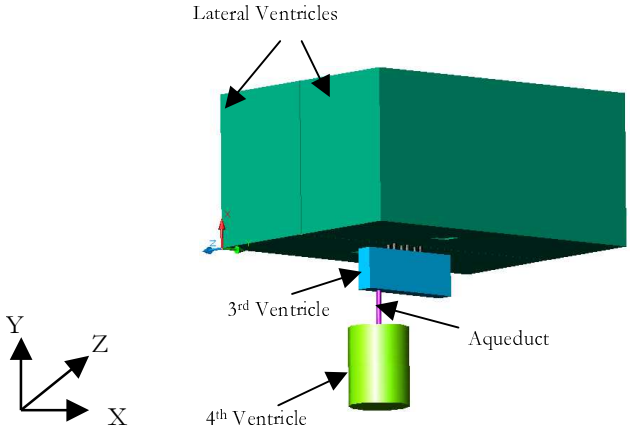


*Fig. 2. The3-D simplified model of the ventricular system.*

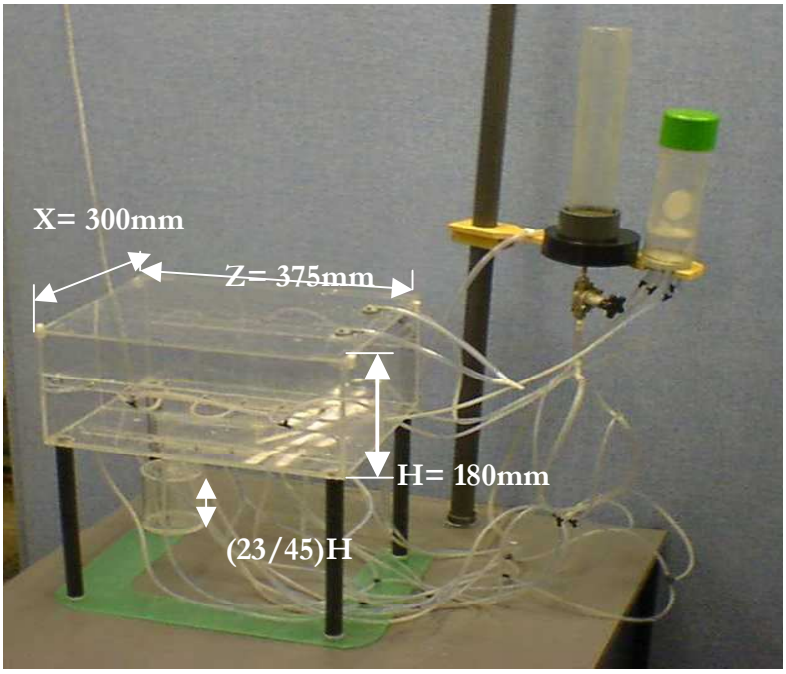


*Fig. 3. The simplified physical model of the ventricular system*

The physical model shown in figure 3 is made from Perspex of 3 *mm* thickness. The choroids plexus are modelled as small 3-*mm* diameter holes drilled in the bottom of each lateral ventricle. Each lateral ventricle has eight small holes. These holes are connected to a main water header tank via small pipes. A pipe is connected to the bottom of the 4th ventricle and acts as the outlet. The inlet and outlet flows are controlled by mechanical valves adjusted to the header tank and to the outlet pipe. The header tank is connected to a continuous water feeding pipe to maintain the water level constant all times. The water flow rate is calibrated by the outlet valve to keep the flow within the desired range. Thus, the fluid in the ventricular model achieves steady state by allowing the water to enter at constant head and exit at constant flow rate, which allows the flow to develop naturally. The model is placed over a rotating tray to allow

acquisition from different sides without a significant change to the laser sheet and the CCD camera positions. The lower part of the model, which is curved, because of the presence of cylindrical parts, was surrounded by a rectangular box filled with water to get rid of the curvature effect, which results in false or stretched vectors.

## 2.2 Experimental Setup and Procedure

The PIV method had been chosen to study the flow behaviour inside the physical rig, because of its effectiveness. The aim of investigating the CSF flow behaviour in vitro is to obtain instantaneous vector map.

The doubled pulsed Nd: YAG laser (532 nm- a green wavelength) was used as the illumination system, because of its high power that is enough to illuminate small seeding particles, which are microns and sub microns in diameter. Quantel Twin laser system pulsing at 15Hz is used and it is shown in figure 4.

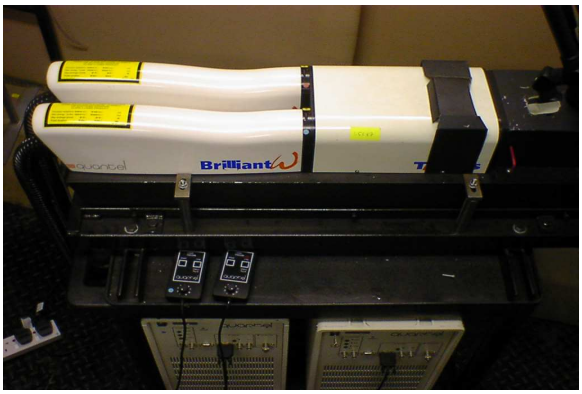


*Fig. 4. T he Quantel system used in the experiments*

The laser beam generated from the Nd: YAG is transmitted through hollow and flexible joints with mirrors mounted at the readily manipulated joints. This assembly has a great flexibility as it allows the incoming beam to be deflected from mirror to anther, regardless of the orientation of the joint. An optical head was attached to the arms assembly to obtain a flat laser sheet in the required position. Figure 5 illustrates the arms assembly and the laser optical head.

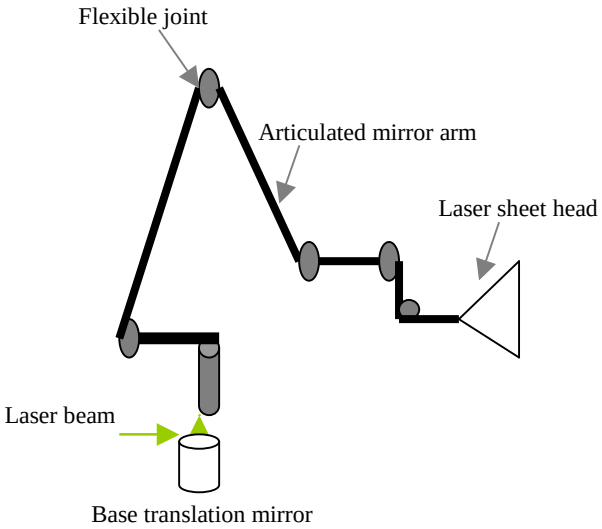


*Fig.5. The arms assembly and the laser optical head*

The acquisitions were recorded by a CCD Kodak MegaPulse ES 1.0/ Type 16 (30 Hz) camera. Thence the acquisitions were stored in the PIV flow Map system 2000 processor.

The choice of seeding particles was a major difficulty despite of the wide variety of the seeding particles that match with the fluid continuum. This is because at the creeping velocity inside the model, the gravitational effect on the seeding

particles is significant. Larger diameter seeding particles 40-100 $\mu m$ precipitates quickly, eventually resulting in low density seeding particles in the interrogation area. The trick is in compromising between particles large enough to give good light scattering and small enough to match with the continuum and have the minimum gravity effect. After testing a selection of seeding particles of different diameters and densities, the Polyamides seeding particles (PSP-20), 20 $\mu m$ diameter and 250g are found to be the best match with the water continuum. These particles are made of a porous matter that allows the continuum fluid to fill in and thence become buoyant and faithfully follow the continuous medium flow pattern.

The Flow Map software 3.21 is used to post-process the acquired images. The flow rate was calibrated to 2395.6 *ml/day*, which equals to 499*ml/day* for the normal range. This is very close to the maximum flow rate which is 2400 *ml/day* for the model and 500 *ml/day* for the actual flow rate. The maximum flow rate has been chosen to speed up the flow and to maintain the longest time before the gravity effects start to be more significant, sine the more dynamic flow maintains better mixing with the seeding particles. After calibrating the camera and the laser sheet in the requested positions, the laser was fired externally using the PIV Flow Map software, which is synchronised with the camera and the laser device. Around 40-70 images are taken at each firing. Single frame images are taken as the flow is slow and the double frame is not needed in this particular case. The idea of taking more images is to give the particles enough time to move, so the correlation will be representative to the flow speed. The time between pulses is between 6-50 ms depending on the investigated location; where the flow is anticipated to be quicker the time between pulses is made shorter. Actually, different timing scales for each plane are done to compromise between them and to select the most representative vector maps.

## 2.3Experimental Results

The rig is divided into several planes in the X and Z directions to scrutinise the flow at the anticipated critical zones inside the model. These anticipated critical zones are over the inlets in the lateral ventricles, over the Foramens of Monro (F.O.M) exits in the lateral ventricles, over the aqueduct in the 3rd ventricle, under the F.O.M exits in the 3rd ventricle, at the middle of the aqueduct and the 4th ventricle. Other less important locations are also investigated. In the lateral ventricles it is found that highest velocity occurs over the inlets and there is a recirculation motion in the low velocity areas, such as the areas next to the walls. The velocity maps that were obtained from the planes over the inlets show that the flow at the top of the plane is directed downwards, but the flow over the inlets has a higher speed and it travels upward with an angle, which then bends and recirculates near the wall. Figure 6 shows a plane over the 1st inlet in the lateral ventricle illustrating the visualisation view, and the laser sheet location with respect to the total Z dimension of the rig that is equal to 375.76 mm.

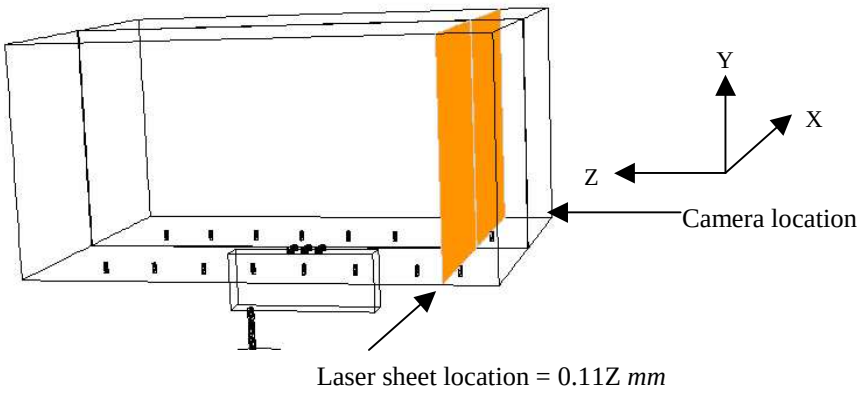


*Fig.6. A plane over the 1st inlet in the lateral ventricle.*

Figure 7 shows the velocity map in the plane indicated in figure 6.

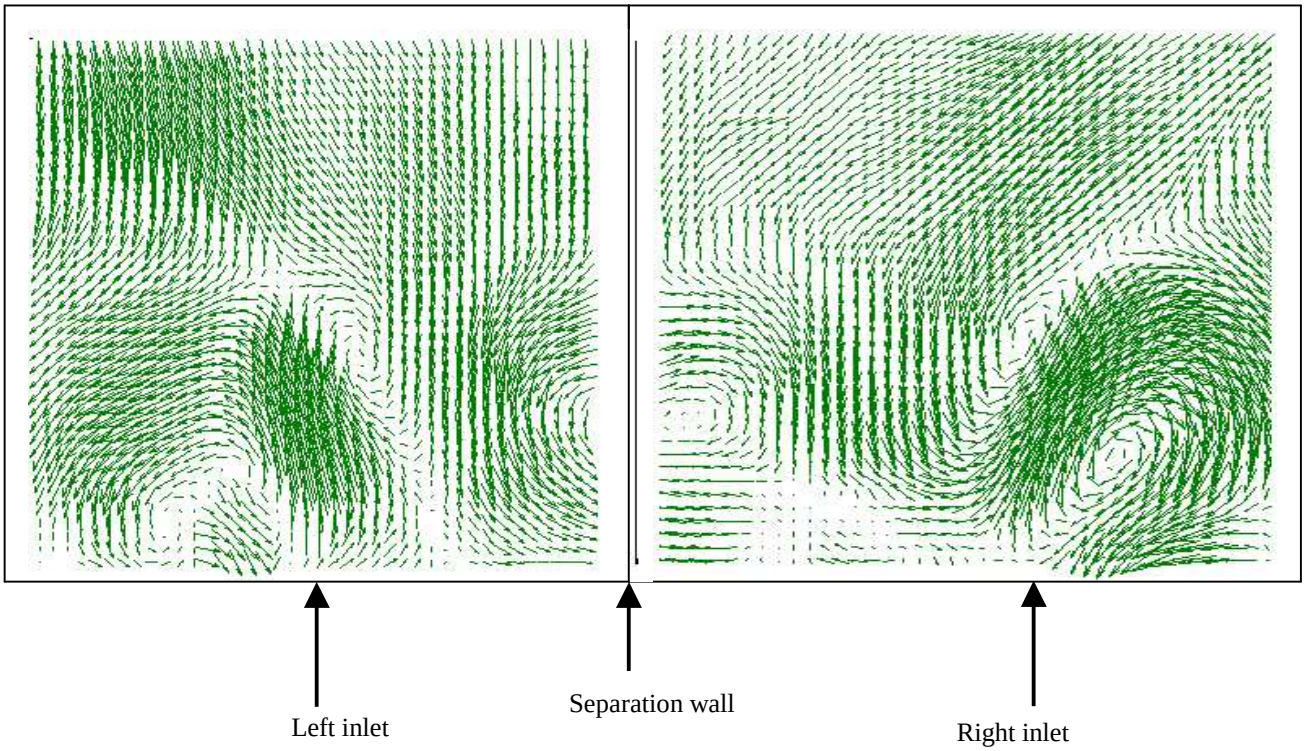


*Fig.7. A Velocity vector map at a plane over the 1st inlet in the lateral ventricle*

It is clear from figure 7 how the flow recirculates near the walls, especially near the separation wall, where the velocity is expected to be the minimum in the plane. The average velocity in the inlets plane is 0.5 *mm/s* at each inlet plane. This recirculation motion is also clear when a dye with properties matching water is injected to trace the flow inside the model. Figure 8 demonstrates the dye recirculation motion injected in the same plane shown in figure 6.

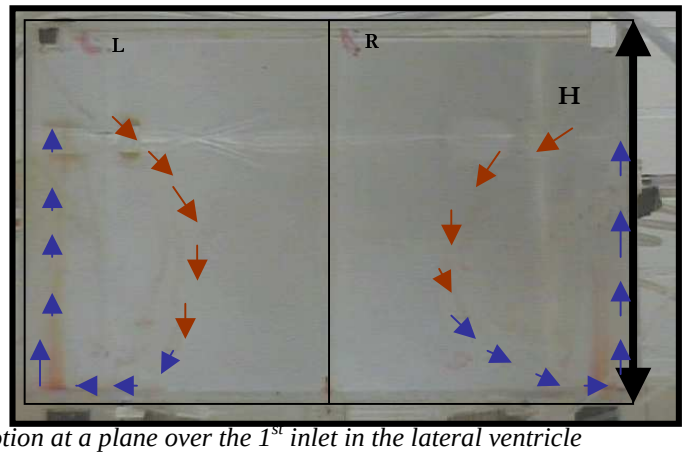


*Fig.8. Dye recirculation motion at a plane over the 1st inlet in the lateral ventricle*

The CFD results reveal that the highest velocity in the lateral ventricles occurs over the inlets, but the CFD vectors are not showing the recirculation motion clearly unless the relatively high velocity vectors clipped, which also will not give a clear picture of the entire flow vector map. The inlets are also visualised from the side, so all the inlets appear in the same plane. In fact, the entire plane is divided into smaller interrogation areas equals to each other to map all the inlets clearly. These small interrogation areas are then joined together to form the whole plane. This method has the advantage of focusing on each two inlets separately, but joining the small interrogation areas together results in losing some information at the interface of the area being joined. However, the aim is to show the inlets effect on the flow and the recirculation resulting from that. The inlets closer to the wall are not noticeably discrete as the inlets in the middle due to the wall effect on the accelerated particles that hit the wall and slow down there, eventually causing a recirculation motion. This explains the presence of dead areas in the ventricular system in the zones far from the active CSF flow such as near the F.O.M exits and the aqueduct. The two lateral ventricles show the same results, the left lateral ventricle plane

vector map is shown in figure 9b and its location is exhibited by figure 9a. The plane location in figure 9a is with respect to the total X dimension of the lateral vetricles, which is 294 *mm*.

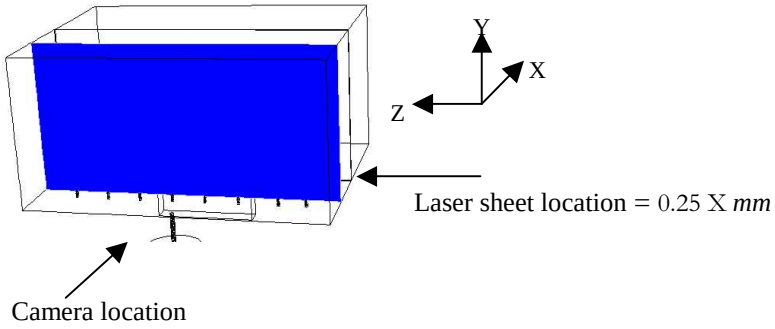


*Fig.9a. A plane over the inlets in the left lateral ventricle*

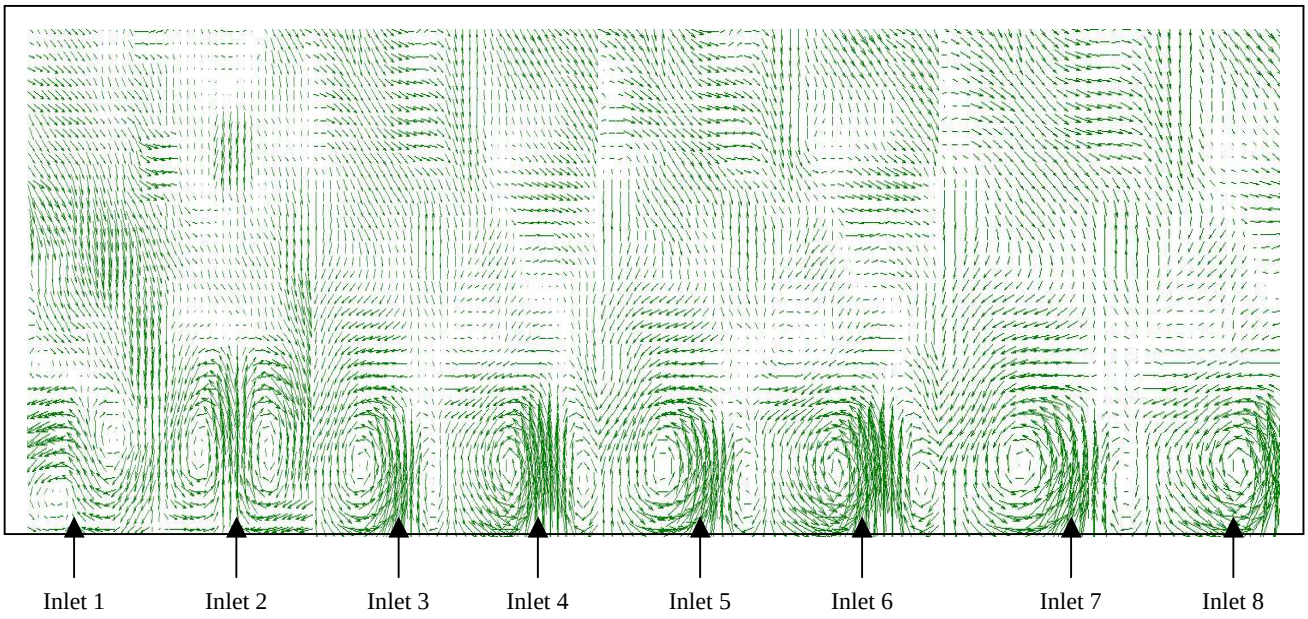


*Fig.9b. Velocity vectors in the plane shown in figure 9a.*

The average velocity in this plane is 0.47 *mm/s*, which is very close to the velocity average in the plane illustrated in figure 7. The slight difference between the plane in figure 7 and the plane in figure 9b is because the plane in figure 9b includes more details of slow flow areas. The PIV study also gives an interesting vector map of how the flow rushes into the F.O.M as well as the average velocity magnitude there. It indicates that the F.O.M is an acceleration zone. Figure 10a is representing the F.O.M plane with a square surrounding the interrogation area of interest.

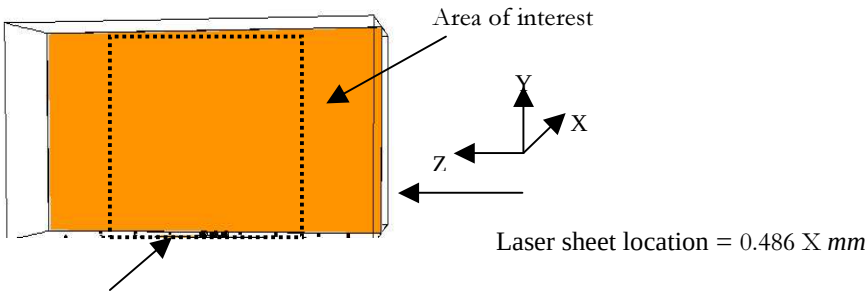


*Fig.10a. A plane over the F.O.M in the left lateral ventricle*

In Figure 10 the laser sheet location is related to the total X dimension of the rig which is 294 *mm*. Figure 10b gives the velocity vectors at the plane shown in figure 10a.

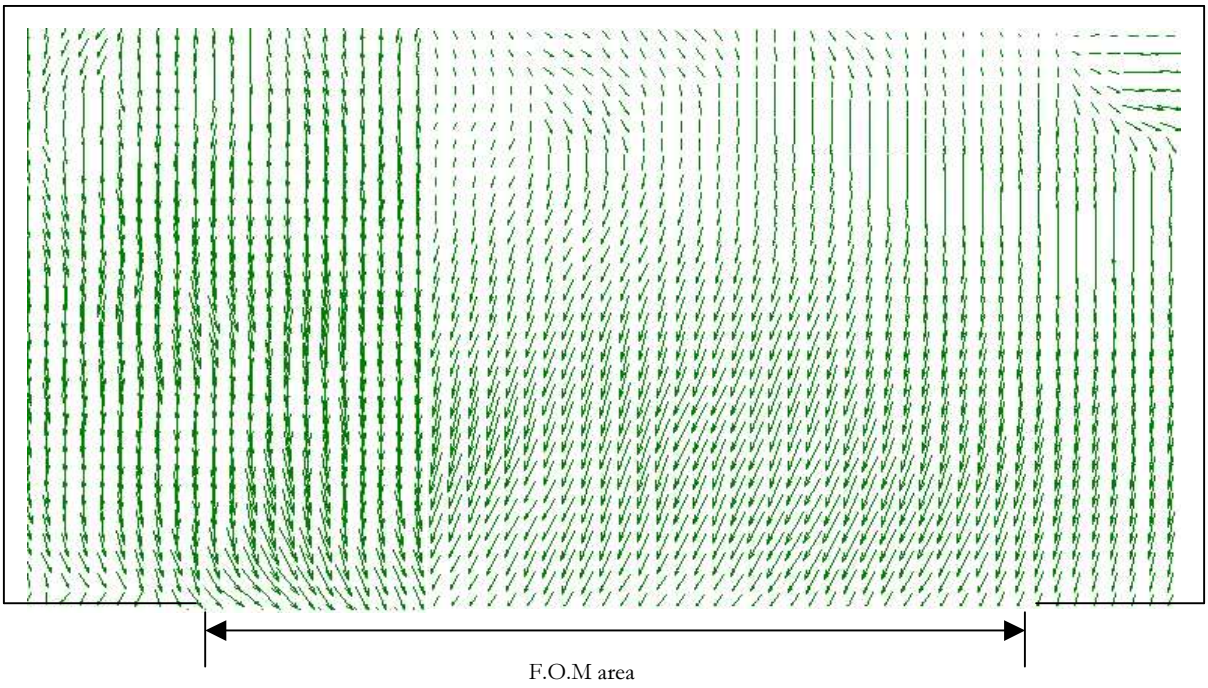


*Fig.10b. Velocity vectors in the plane shown in figure 10a.*

It is clear from figure 10b how the flow is directed to the F.O.M exits. The average velocity magnitude recorded at the F.O.M exit is 0.6 *mm/s*. Actually, if the interrogation area is extended to include all the plane with the walls, the average velocity will be less than that, but more focus is needed on the F.O.M area as well as to show that the flow is accelerated there. Generally the inlets have a velocity magnitude higher than the F.O.M. The CFD study shows nearly the same pattern over the F.O.M exits as indicated in figure 11.

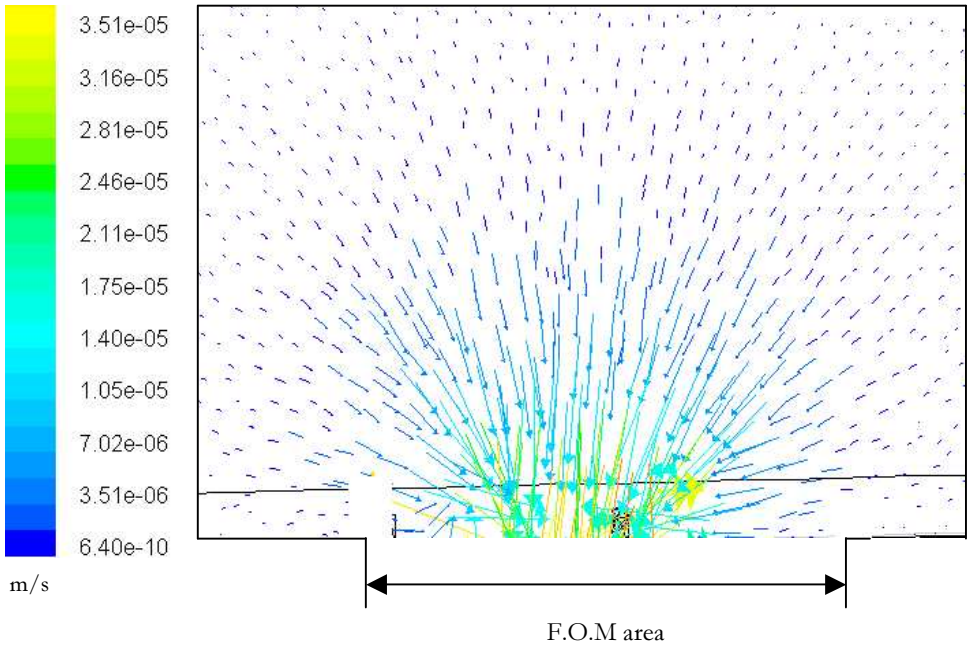


*Fig.11. CFD velocity vectors in the plane shown in figure 10a*

In the lower part of the model, the PIV study shows that in the 3rd ventricle as the flow enters via the F.O.M it tends to take a 90º turn to the rear direction, resulting in a lower velocity zones in some parts of the 3rd ventricle. This finding validates the CFD results in the 3rd ventricle. The planes close to the aqueduct and the F.O.M have the highest velocity, while the planes closer to the walls have a dying velocity. Figure 12a shows the plane over the aqueduct with the laser sheet location which is related to the total X dimension of the 3rd ventricle, namely 20.5 *mm*. Figure 12b, indicates the velocity vectors in the plane shown in figure12a

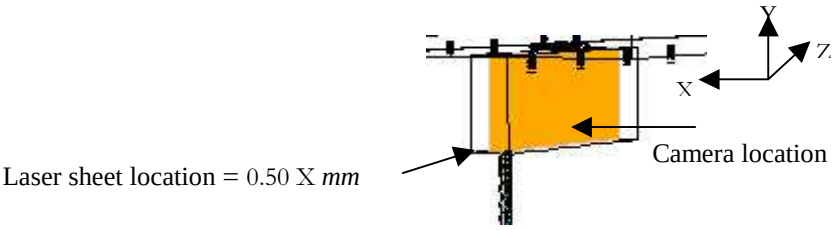


*Fig.12a. A plane over the aqueduct in the 3rd ventricle*

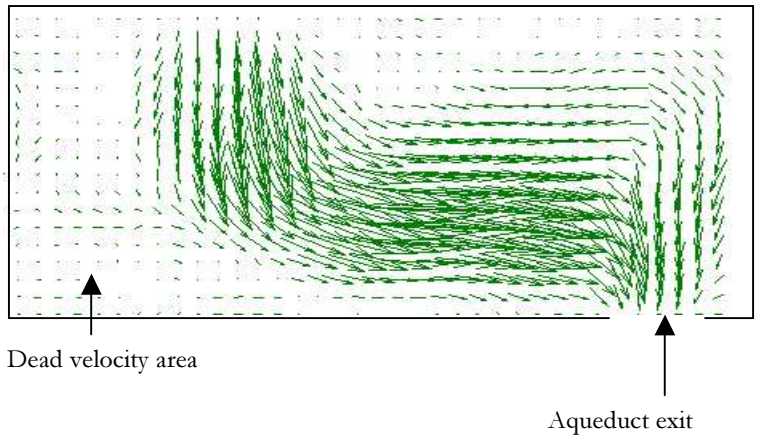


*Fig.12b. Velocity vectors in the plane shown in figure 12a.*

The average velocity magnitude in the plane shown in figure 12a is 0.35 *mm/s*. The CFD results go very well with the PIV vector map as illustrated in figure 13. Both plots show the throttling effect of the corner recirculation and the low resistance path the flow has taken.

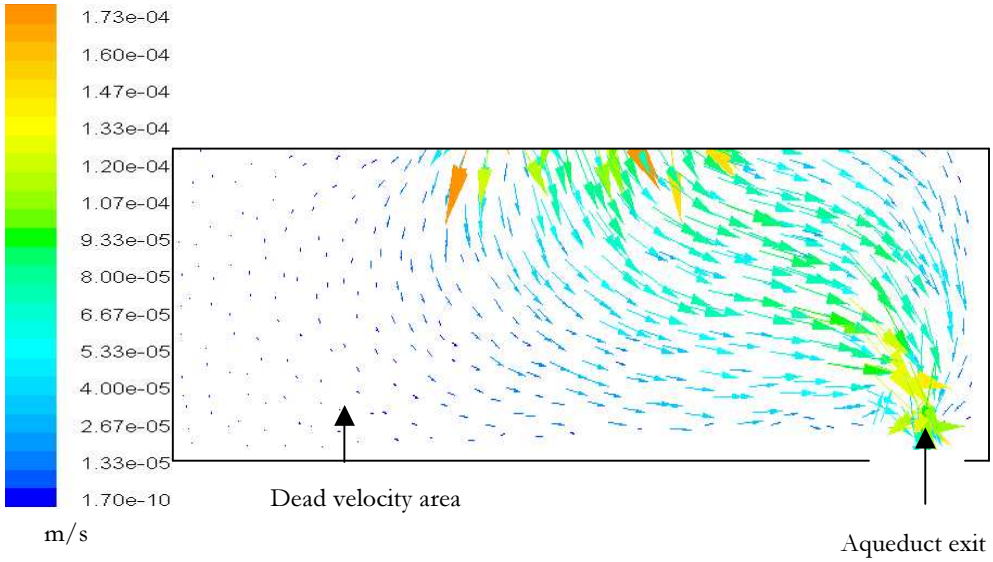


*Fig.13. CFD velocity vectors in the plane shown in figure 10a*

The flow in the aqueduct is found to be not only directed downwards, but it has a swirling motion. Although the aqueduct is a symmetric cylinder, it is visualised from different angles to prove the consistency of the swirling motion. The plane of figure 12a applies also on the aqueduct since it cuts through its centre. Due to the small dimensions of the aqueduct that is 5.6 mm for the scaled rig. It has only been possible to investigate the flow in the middle plane. The average velocity magnitude in the aqueduct plane is found to be 0.9 *mm*/s, which is the highest in the intact model. Figure 14, shows the velocity vectors map in the aqueduct.

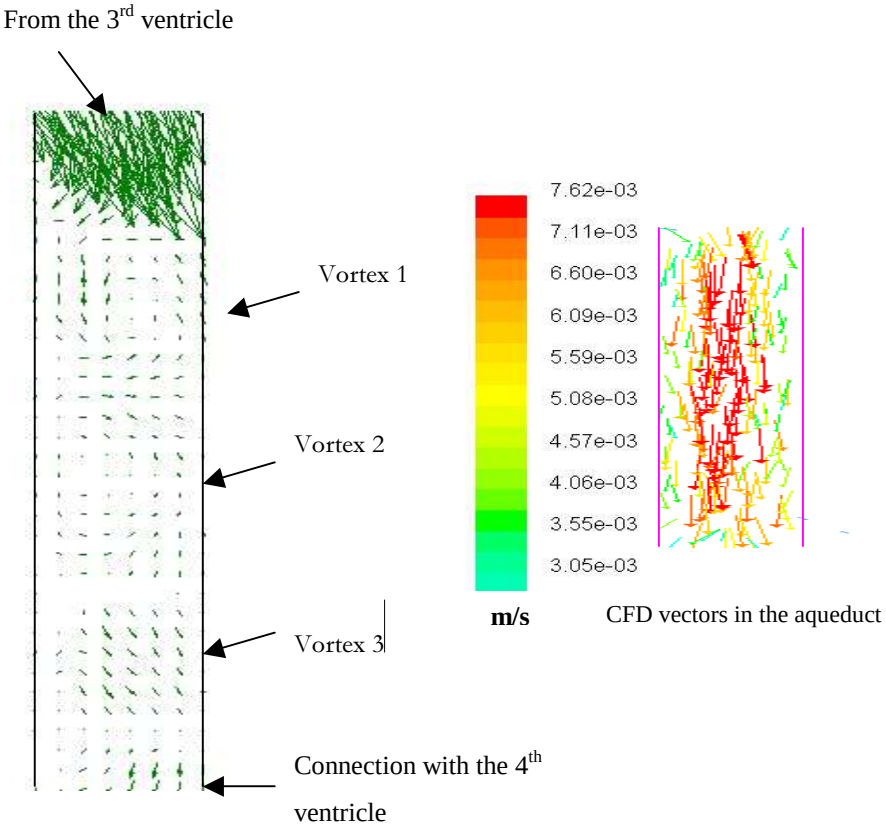


*Fig.14. PIV velocity vectors in the middle plane of the aqueduct and CFD vectors at the same plane*

It is clear from figure 14 that the highest velocity occurs at the duct's neck, which goes with the CFD findings of the simplified model. The CFD vectors do not show the vortices in the aqueduct clearly as the PIV. This is may be due to the computational simplifications and possibly the mesh, but the CFD still emphasised the prevailing downward motion as well as that the highest velocity in the entire model occurs at the aqueduct's neck. In earlier relevant studies it was found that the bulk flow of significance happens at the aqueduct (Jacobson et al, 1996), which also goes with the PIV finding about the occurrence of the highest velocity in the aqueduct's neck. In the 4th ventricle as soon as the flow enters the chamber it diffuses there and its velocity decreases. Recirculation motion was also detected. Figure 15a shows the middle plane of the aqueduct, which is in fact a continuation of the plane shown in figure 12a that cuts through the aqueduct since the aqueduct and the 4th ventricle are co-centric. The laser sheet location in figure 15a is correlated to the 4th ventricle diameter which is 73.2 *mm* for the scaled up rig.

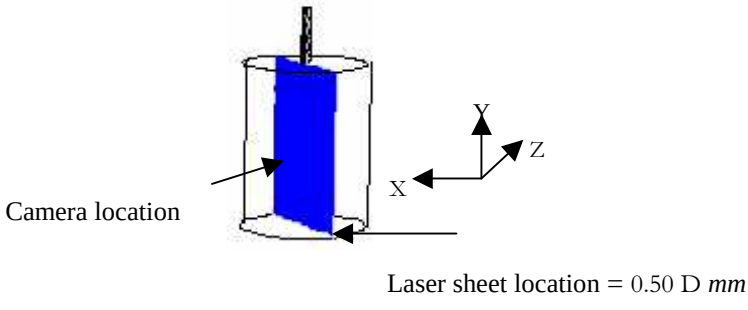


*Fig.15a. the middle plane of the 4th ventricle*

Figure 15b is gives the flow vector map in the plane shown in figure 15a. The average velocity there is 0.18*mm/s.*

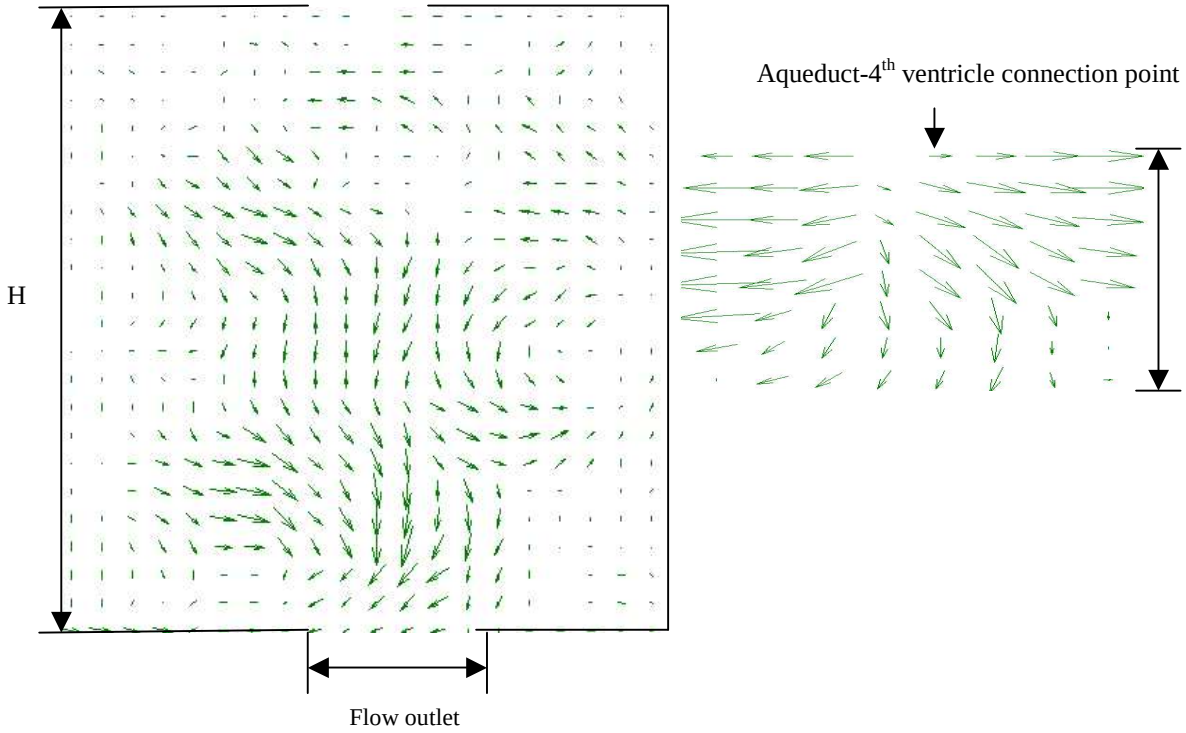


*Fig.15b. PIV velocity vectors in the middle plane of the 4th ventricle with magnification of the point of connection with the aqueduct*

The CFD vector map of the same plane shows also the downward motion and the recirculating flow only in the upper half of the 4th ventricle. As the lateral ventricles, showing the entire map will not be representative, since the highest vectors in the 4th ventricle inlet are dominant, but clipping them will result in missing information in a significant part of the 4th ventricle

## 3. CONCLUSIONS

The PIV has proven its utility in predicting the flow pattern of a creep flow. More than twenty acquisitions should be taken to obtain a representative correlation of the creep flow with a time margin between pulses in the range of 6-50m/s, which is preferable for an *mm/s* or sub *mm/s* velocity order flows (creeping flow).

The seeding particles choice for the creep flow is not trivial because of the greater gravity effect on creep flows than it is on higher velocities flows. The polyamide (PSP-20), 20 $\mu m$ diameter and 250g were the best choice with water continuum of a creeping nature because of their porous nature that keeps the particles buoyant and following the continuum pattern faithfully for longer.

The PIV results in the simplified scaled up physical model emphasised the presence of a recirculation motion everywhere in the model, especially in the areas of comparatively slow velocity. This recirculation motion may have a great impact on drug delivery to the central nervous system via the CSF, as it predicts the entrapment areas, where the drug will be kept for a longer time, eventually resulting in a systemic toxicity. The highest velocity in the intact model occurs at the aqueduct's neck. In the lateral ventricles the highest velocity occurs over the inlets and it is also has a relatively higher speed at the Foramens of Monro exits, since the flow is accelerating there.

The PIV results showed a good match with the CFD results as it shows the same flow pattern in the 3rd ventricle and the Foramens of Monro exits. Also the analysis of the velocities at different parts of the ventricular model match in its

findings with the PIV, such as that the aqueduct has the fastest flow, but the CFD values differ from the experimental values, because the CFD solution has been done on a 1:1 model.

**REFERENCES**


Ammourah, S., Aroussi, A. and Vloeberghs, M. (2003). "Cerebrospinal fluid dynamics in a simplified model of the human ventricular system". Proc. 11th annual conference of CFD, 26-29 May, Vancouver BC Canada

Aroussi, A., Zainy, M. and Vloeberghs, M. (2000). "Cerebrospinal fluid dynamics in the aqueduct of Sylvius". International symposium of flow visualisation, 95, pp. 1-11

Bloomfield, I, Johnston I and Bilston (1998). "The effect of biochemical composition on cerebrospinal fluid viscosity". ASME

Jacobson, E., Fletcher, D., Morgan, M. and Johnston, I. (1996). "Fluid dynamics of the cerebral aqueduct". Pediatric Neurosurgery, 24, pp. 229-236

Proescholdt, M., Hutto, B., Brady, L. and Herkenham, K (2000). "Studies of cerebrospinal fluid flow and penetration into brain following lateral ventricle and cisterna magna injections of the tracer (14c) inulin in rat. Neuro scince, 95, pp. 577-592

Siegal, T. & Zylber-Katz, E.(2002). "Strategies for increasing drug delivery to the brain". Clin pharmacokinet , 41, pp. 171-186

Vloeberghs, M., Towe, J. Zainy, M. Cartmill, M. and Aroussi, A. (2000). "A parametric study of the cerebrospinal fluid flow in the human ventricular system". Child's Nervous Syst, 16, pp. 535

Yu, S., Zaho, J., Chan, W., Chua, L. and Hui, F. (1997). "Steady and pulsatile flow characteristics in cerebrovascular aneurysm. Part2: A particle image Velocimetery study". Proc. 9th Int conference on biomedical engineering, 3-6, Singapore

Zainy, M., (2002). "Hydrodynamic modeling of the cerebrospinal fluid motion within the human ventricular system", Ph.D. Thesis, University of Nottingham, Nottingham-UK